Available online at www.sciencedirect.com
SCIENCE DIRECT®
ELSEVIER
Journal of Applied Geophysics 55 (2004) 61–76
JOURNAL OF APPLIED GEOPHYSICS
www.elsevier.com/locate/jappgeo

Application of ground-penetrating radar, digital optical borehole images, and cores for characterization of porosity hydraulic conductivity and paleokarst in the Biscayne aquifer, southeastern Florida, USA ☆

Kevin J. Cunningham*

U.S. Geological Survey, Water Resources Discipline, 9100 NW 36th Street, Suite 107, Miami, FL 33178, USA

Abstract

This paper presents examples of ground-penetrating radar (GPR) data from two study sites in southeastern Florida where karstic Pleistocene platform carbonates that comprise the unconfined Biscayne aquifer were imaged. Important features shown on resultant GPR profiles include: (1) upward and lateral qualitative interpretative distribution of porosity and hydraulic conductivity; (2) paleotopographic relief on karstic subaerial exposure surfaces; and (3) vertical stacking of chronostratigraphic high-frequency cycles (HFCs). These characteristics were verified by comparison to rock properties observed and measured in core samples, and identified in digital optical borehole images. Results demonstrate that an empirical relation exists between measured whole-core porosity and hydraulic conductivity, observed porosity on digital optical borehole images, formation conductivity, and GPR reflection amplitudes—as porosity and hydraulic conductivity determined from core and borehole images increases, formation conductivity increases, and GPR reflection amplitude decreases. This relation allows for qualitative interpretation of the vertical and lateral distribution of porosity and hydraulic conductivity within HFCs. Two subtidal HFCs in the uppermost Biscayne aquifer have significantly unique populations of whole-core porosity values and vertical hydraulic conductivity values. Porosity measurements from one cycle has a median value about two to three times greater than the values from the other HFC, and median values of vertical hydraulic-conductivity about three orders of magnitude higher than the other HFC. The HFC with the higher porosity and hydraulic conductivity values is shown as a discrete package of relatively low-amplitude reflections, whereas the HFC characterized by lower porosity and hydraulic-conductivity measurements is expressed by higher amplitude reflections. Porosity and hydraulic-conductivity values measured from whole-core samples, and vuggy porosity identified on digital borehole images from shallowing-upward, peritidal HFCs show that the highest porosity occurs at the base of the cycles, moderate porosity at the middle of the cycles, and lowest porosity occurs at the top of cycles. Hydraulic conductivity is also highest at the base of the peritidal cycles and lowest in the middle to upper parts of cycles. This change in porosity and hydraulic conductivity from bottom to top is visible as an upward variation in reflection amplitude on GPR profiles—lowest amplitudes at the base and highest at the cycle tops. This study demonstrates that GPR can be used to show the qualitative distribution of porosity and hydraulic conductivity within a cycle-stratigraphic framework composed of carbonate HFCs. The distribution of porosity and

☆ The use of brand names in this paper is for identification purposes only and does not constitute endorsement by the author, the U.S. Geological Survey, or the Journal of Applied Geophysics.

* Tel.: +1-305-717-5813; fax: +1-305-717-5801.
E-mail address: kcunning@usgs.gov (K.J. Cunningham).

0926-9851/$ - see front matter
doi:10.1016/j.jappgeo.2003.06.005

hydraulic conductivity within HFCs is related to depositional textures. The upward and lateral patterns of the rock facies within the HFCs can be translated to geophysical-log properties and radar facies configurations that could aid in interpretation and prediction of ground-water flow through a carbonate aquifer.

Keywords: Ground-penetrating radar; Porosity; Biscayne aquifer; Carbonates; Karst; Southeastern Florida

1. Introduction

Ground-penetrating radar (GPR), combined with a precisely defined cycle stratigraphy from cores and digital borehole images, and the detection of vuggy porosity from digital borehole images of near surface karst limestone, can provide a robust visualization of karst aquifer architecture, encompassing the spatial distribution of aquifer bodies, barriers, conduits, and connectivity. Calibration of high-resolution borehole data to GPR attributes for complex karst carbonate lithologies requires continuously cored boreholes and digital-image logs. The high-resolution study of the shallow, karstic Biscayne aquifer serves as a guide for developing improved and more realistic geology-based karst-carbonate aquifer models.

Although the geologic application of GPR is most common for siliciclastic strata (e.g., Beres and Haeni, 1991; Smith and Jol, 1992; van Overmeeren, 1998) and crystalline rocks (e.g., Grasmueck, 1996; Lane et al., 2000), its use in karst-carbonate rocks is becoming more common (Ballard, 1983; Beck and Wilson, 1988; Barr, 1993; McMechan et al., 1998; Beres et al., 2001; Cunningham and Aviantara, 2001). GPR has been applied to near-surface carbonate rocks, but the combined use of GPR and digital borehole images is a new application (Cunningham and Aviantara, 2001). No published examples have been found that demonstrate the use of GPR to delineate porosity within a carbonate high-frequency cycle stratigraphy. Other lithologic and hydraulic features that can be inferred from GPR profiles include sediment types and thickness (Beres and Haeni, 1991), karst features (Barr, 1993; McMechan et al., 1998), subaerial-exposure surfaces (Kruse et al., 2000), and depth to water table and clay beds (Johnson, 1992; Barr, 1993). McMechan et al. (1998) used GPR to image a near-surface paleocave system in the Lower Ordovician Ellenberger dolomites in central Texas. Martinez et al. (1998) showed that small-scale (less than 0.01 m) lithologic heterogeneity could be identified with GPR imaging of Pennsylvanian cyclic limestone outcrops in Kansas. The lithologic heterogeneity, which affects permeability, can provide quantitative data for use in fluid-flow modeling. Dagallier et al. (2000) showed that GPR could be used to identify the internal organization of lithologic units within Jurassic limestone in France. Kruse et al. (2000) have shown that GPR can be effective in mapping the altitude and structure of shallow limestone cap rock in the prairie, cypress swamp, and hardwood hammock of the Fakahatchee Strand State Preserve in southwestern Florida. Beres et al. (2001) demonstrated that GPR is an excellent tool for identifying and delineating shallow subsurface cavities in karstified Jurassic limestone in Switzerland.

2. Purpose and scope

The purpose of this paper is to demonstrate how the combined use of GPR, borehole-geophysical logs, and continuously drilled cores can be used to characterize the spatial distribution of porosity and identify karst features within shallow carbonate aquifers. In this paper, it is shown that GPR profiles combined with cores and digital optical borehole image logs can contribute powerfully to characterizing hydrogeologic properties of shallow karst-carbonate aquifers. This investigation demonstrates the effective use of the relation between porosity and high-frequency carbonate cycles and amplitude of reflections in GPR profiles, to characterize a karst-carbonate aquifer. Results from this study have improved the understanding of the distribution of porosity in young (Pleistocene) platform carbonates that comprise an unconfined surficial aquifer.

GPR profiles and data from test coreholes were collected at two sites, the north-central Miami-Dade site and the Rocky Glades site, in southeastern Florida (Fig. 1). To enhance the data set, whole-core porosity

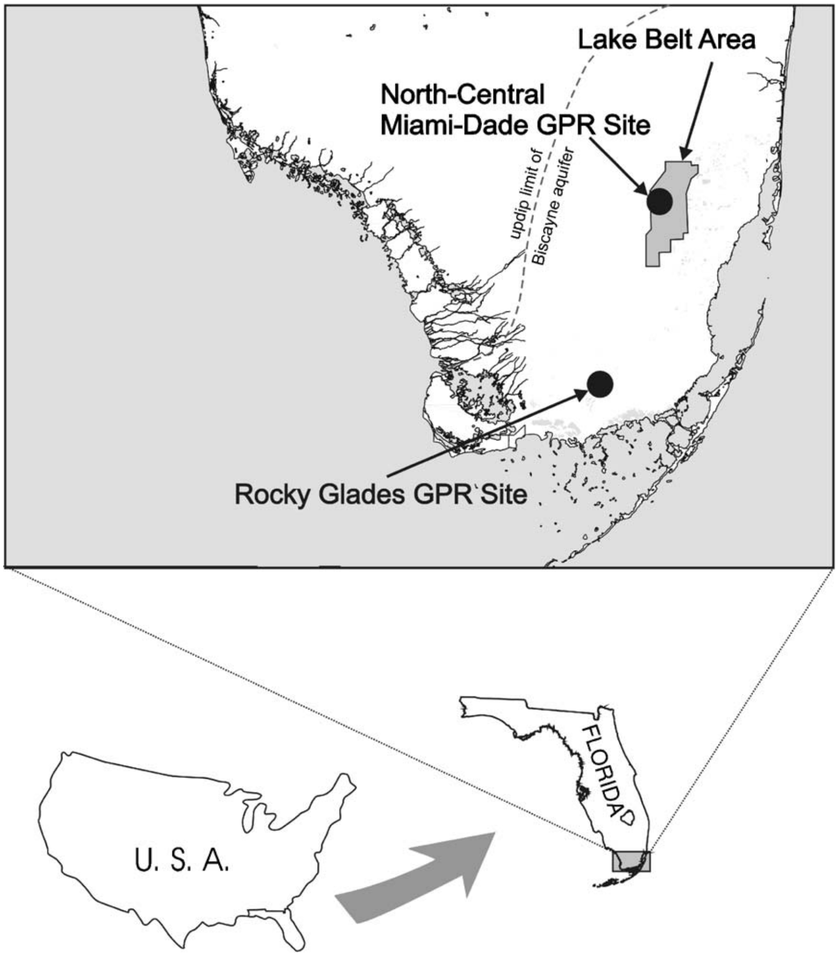

Fig. 1. Map of locations of the north-central Miami-Dade and Rocky Glades ground-penetrating radar (GPR) sites, and the Lake Belt Area.

values were used from ongoing research of the surficial aquifer in the Lake Belt Area (Cunningham and Aviantara, 2001), which includes the north-central Miami-Dade site (Fig. 1).

3. Methods

3.1. GPR surveys

Two types of GPR field surveys were conducted for this project: (1) continuous measurement common-offset reflection surveys and (2) common midpoint (CMP) velocity surveys (Annan and Davis, 1976; Davis and Annan, 1989). The common-offset reflection surveys were performed to produce two-dimensional profiles of the GPR reflections, and the CMP surveys were used to calculate radar velocities propagating through the solid and fluid material comprising the Biscayne aquifer. All GPR data was collected using a Geophysical Survey Systems (GSSI) SIR™ System-10A+ with a dual 100-MHz antenna array. The common-offset reflection surveys were collected while towing the antennas 17 m behind a truck at a rate of about 0.8 km/h. The separation between the center points of the antennas was 89 cm. Velocities were calculated by correlating depths to reflectors, which could be determined from positive correlation with corehole lithologies and the CMP surveys. Processing included a horizontal filter pass and, for some GPR profiles, a constant-velocity migration of the continuous survey data using GSSI RADAN™ for WinNT software. Identification of GPR reflection amplitudes also was accomplished using the software GSSI RADAN™. Interpretations of profiles were made using the RADAN™ for WinNT software and RADAN™-to-bitmap conversion utility. The descriptions of radar-reflection patterns are consistent with patterns described for seismic profiles by Mitchum et al. (1977).

3.2. Drilling, borehole geophysical logs, and whole-core porosity

Seven test wells were drilled to verify results from GPR surveys. Four test coreholes were drilled at the north-central Miami-Dade site (Fig. 1). Two test coreholes and one rotary roller-bit test well were drilled at the Rocky Glades site (Fig. 1). Borehole-geophysical logs were collected by the U.S. Geological Survey (USGS) for all seven test wells and included conductivity, natural gamma ray, caliper, and digital borehole image logs. The digital borehole image logs were run using either a RaaX™ Borehole Image Processing System (BIPS™) or an ALT OBI-40™ digital optical logging tool in the test wells filled with clear, ambient freshwater. Sixty-nine whole-core porosity measurements were made on samples of core drilled at both the north-central Miami-Dade and Rocky Glades GPR sites, and on samples from other test coreholes drilled throughout the Lake Belt Area (Fig. 1). Air-permeability values were converted to hydraulic conductivity values using a factor of 1 millidarcy equals 9.67×10^{-9} m/s.

4. Cycle stratigraphy

The spatial distribution of vuggy porosity in the Pleistocene carbonate rocks of the Biscayne aquifer is controlled mostly by the distribution of depositional textures, which is best described by a stratigraphic framework comprised of high-frequency cycles (HFCs). Using a modified definition by Lucia (1999), the HFC is a chronostratigraphic unit composed of an unconformity-bounded succession of genetically related textures contained in beds or bedsets. The upper and lower bounding surfaces of the HFC are surfaces of subaerial exposure caused by a relative fall in sea level.

Two types of HFCs are present in the Biscayne aquifer. One is a subtidal cycle formed by vertical

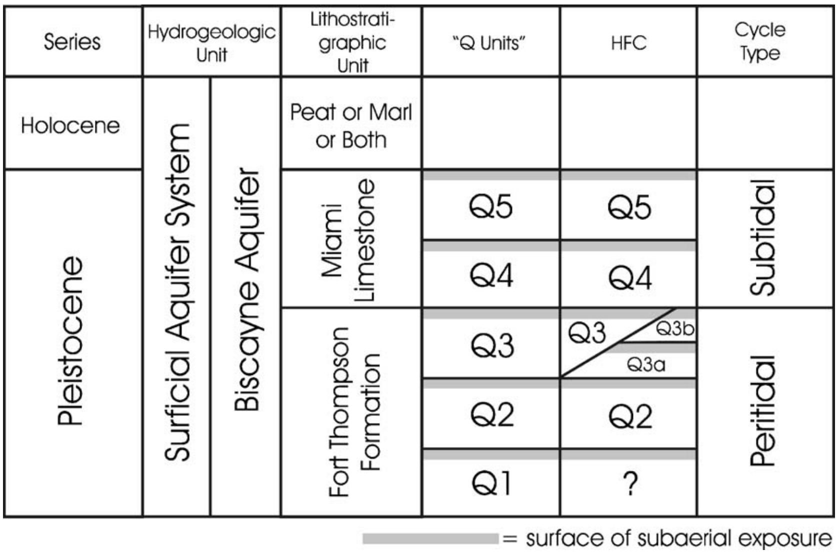

Fig. 2. Shallow time stratigraphic units, hydrostratigraphy (Fish and Stewart, 1991), lithostratigraphy (Causaras, 1987), "Q units" of Perkins (1977), and high-frequency cycles (HFC) used in this report for southeastern Florida.

aggradation of high-energy shoals or shallow-marine, peloidal, highly burrowed sand flats. The Miami Limestone contains two unconformity bounded subtidal HFCs (Fig. 2). The second type of HFC, a peritidal cycle, is composed of a succession of depositional textures that decrease in grain size upward, that shallow upward, and is capped by a tidal-flat deposit or freshwater limestone or a stacking of both. Three peritidal HFCs are recognized in the upper part of the Fort Thompson Formation (Fig. 2). The delineation of HFCs in the lower part of the Fort Thompson is currently under investigation. The "Q" terminology of the HFCs is modified from Perkins (1977), who first recognized that the Miami Limestone and Fort Thompson Formation of south Florida are composed of five unconformity-bounded, time-stratigraphic marine units (Fig. 2). These units were informally termed, from oldest to youngest, Q1 through Q5 (Q for Quaternary). Fig. 2 shows the relation between the "Q units" of Perkins (1977) and the HFCs of this study.

5. Results of GPR surveys

5.1. Rocky glades site

At the Rocky Glades site (Fig. 1), the radar reflections from the Q5 subtidal HFC typically have poor horizontal continuity or hummocky configurations (Fig. 3). These reflection patterns image highly bioturbated, massive beds (without well-defined bedding planes) composed of pelmoldic grainstone and packstone that have very high porosities and hydraulic conductivities (Figs. 4–6). The reflections of the Q5 HFC are mostly lower amplitude than reflections in the underlying uppermost limestone of the Q4 HFC (Fig. 3). Amplitude analysis demonstrates that a reflection representing the base of the Q5 HFC has substantially lower amplitude than amplitudes of the top layers of the Q4 HFC (Fig. 7a). The basal reflection of the Q5 HFC averages about 6 decibels (dB) lower than amplitudes at the top of the Q4 HFC

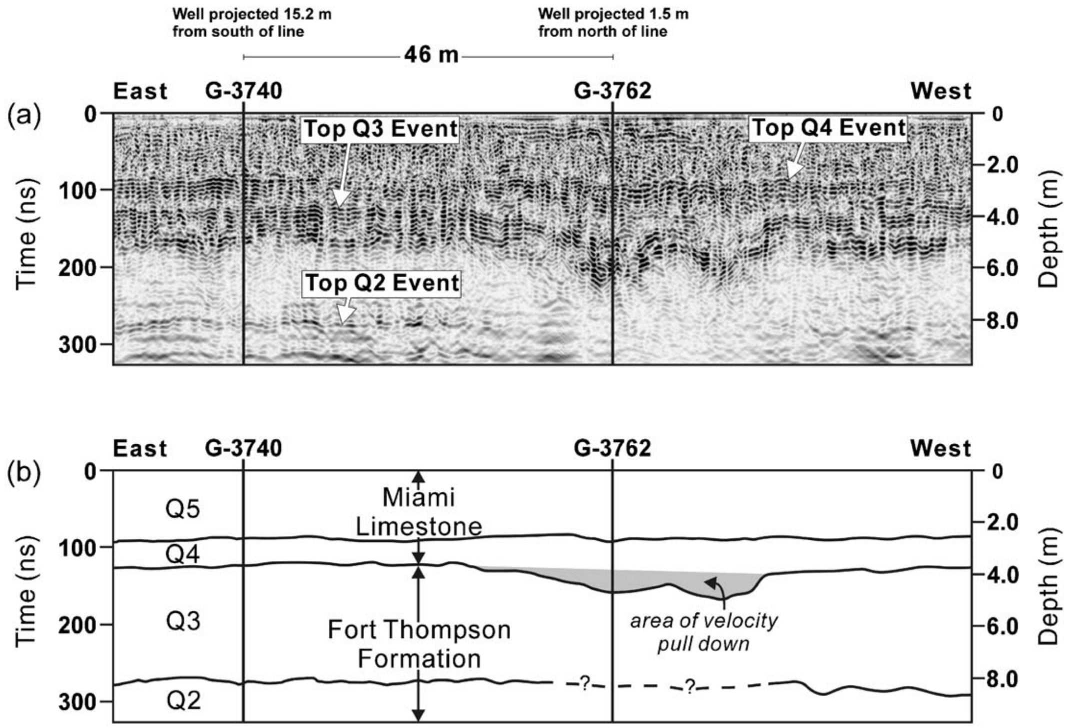

Fig. 3. GPR line 286 at the Rocky Glades site, Everglades National Park. (a) 100-MHz profile across zones of very high porosity in high-frequency cycles Q4 and Q3. A horizontal-filter pass has been applied to the profile. (b) Line drawing of GPR profile. Q5, Q4 and Q3 correspond to the high-frequency cycle stratigraphy shown in Fig. 2.

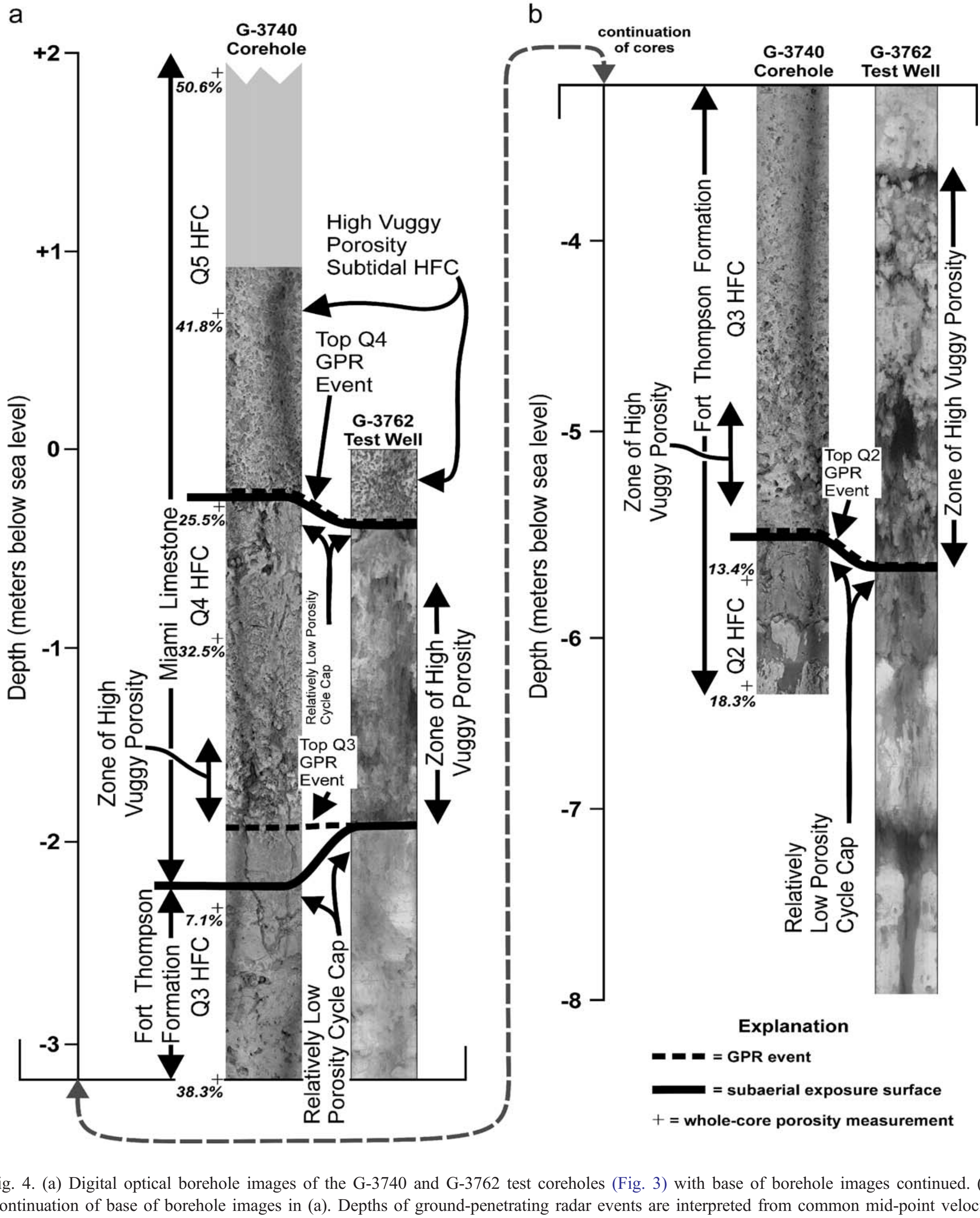

Fig. 4. (a) Digital optical borehole images of the G-3740 and G-3762 test coreholes (Fig. 3) with base of borehole images continued. (b) Continuation of base of borehole images in (a). Depths of ground-penetrating radar events are interpreted from common mid-point velocity surveys and correlation to test-corehole lithology. Zones of relatively high vuggy porosity are shown. HFC = high-frequency cycle.

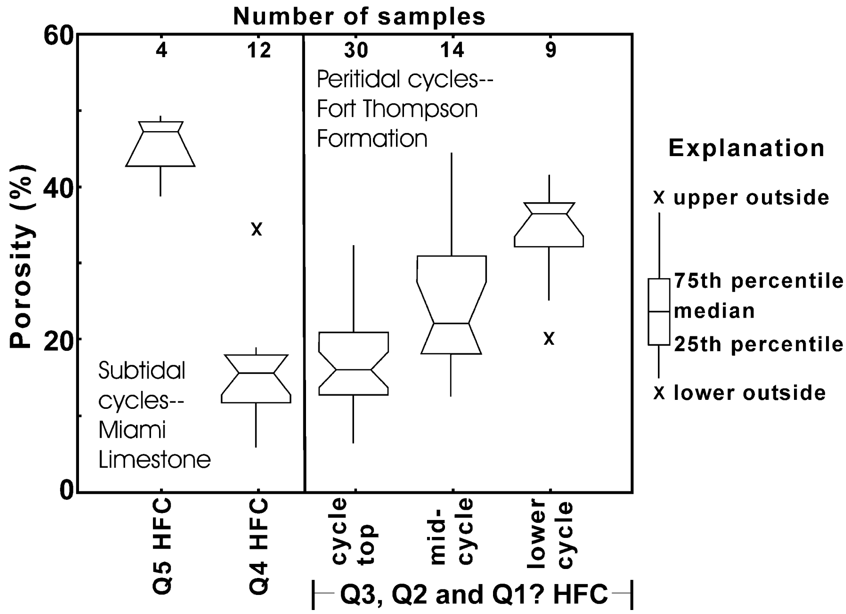

Fig. 5. Box-whisker plots of laboratory-measured porosity of whole-core samples from the Rocky Glades GPR site and Lake Belt Area. In the box plot, the upper and lower quartiles of the data are portrayed by the top and bottom of the polygon, and the horizontal line segment within the polygon represents the median. When comparing the notches on two boxes, if the notches do not overlap, this indicates a difference in the median of porosity populations at about a 95% confidence level. Where there is overlap of notches, there is not a significant difference in the medians. Roughly 99% of the data is contained between the limits of the whiskers and the remaining 1% of the data are plotted as individual points. The plots for the two subtidal high-frequency cycles of the Miami Limestone indicate that the upper Q5 high-frequency cycle (HFC) has significantly higher values of porosity than the lower cycle (Q4 HFC). The three plots to the right indicate that the porosity values within the high-frequency peritidal cycles of the Fort Thompson Formation decreases upward from cycle base to cycle cap.

(Fig. 7a). The relatively low amplitudes of the reflections of the Q5 HFC are consistent with a very high pelmoldic matrix porosity, high solution-enlarged burrow porosity, and high hydraulic conductivity that are characteristic of the Q5 HFC (Figs. 5 and 6). The relatively high reflection amplitudes of the Q4 HFC correlate with a micrite-rich rock fabric that has a characteristically lower porosity and hydraulic conductivity (Figs. 5 and 6). Whole-core porosity values of the Q5 HFC from the Lake Belt Area and Rocky Glades site (Fig. 1) range from 40% to 50%, and values from the Q4 HFC are two to three times lower (Fig. 5). The average median whole-core vertical hydraulic-conductivity value of the Q5 HFC averages about three orders of magnitude higher than the median value from the Q4 HFC (Fig. 6a) and the median whole-core maximum horizontal hydraulic-conductivity value of the Q5 HFC averages about one order of magnitude higher than the median value from the Q4 HFC (Fig. 6b).

The lower amplitudes of the reflections in the Q5 HFC relative to higher reflection amplitudes in the top layers of the Q4 HFC are probably caused by much higher porosities, and thus higher freshwater content in the Q5 HFC. Fig. 8 shows that the formation conductivity of the Q5 HFC is higher than the formation conductivity of the top layers of the Q4 HFC. The attenuation of electromagnetic (EM) waves increases as the electrical conductivity of a medium increases (Lane et al., 2000). Thus, there is an empirical relation between formation porosity, hydraulic conductivity, formation conductivity, and reflection amplitudes—as porosity increases, hydraulic conductivity and formation conductivity increases, and reflection amplitude decreases. This relation is observed throughout the entire vertical and lateral section of the Biscayne aquifer represented in Figs. 3 and 4.

The top of the Q4 subtidal HFC has a relatively low porosity limestone cap and much of the bottom

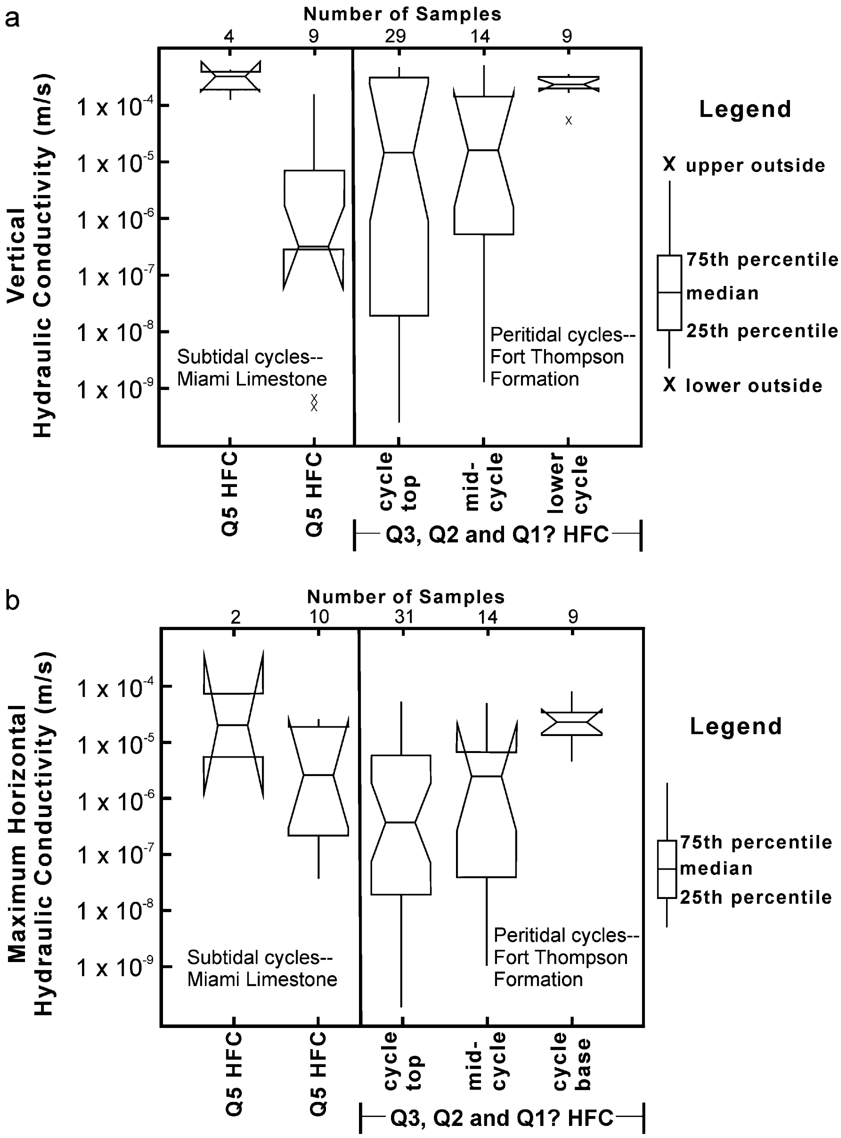

Fig. 6. Box-whisker plots of hydraulic conductivity of most of the same samples displayed in Fig. 5. See Fig. 5 for an explanation of the box-whisker plots. Hydraulic conductivities were calculated from laboratory-measured air-permeability values using a factor of 1 millidarcy equal to 9.67×10^{-9} m/s. (a) Vertical hydraulic conductivity and (b) maximum horizontal hydraulic conductivity.

section of the Q4 HFC is characterized by higher matrix and vuggy porosity (Fig. 4). On the GPR profile shown in Fig. 3, the reflections in the top layers of Q4 HFC have relatively higher amplitude than the reflections in the bottom section of the Q4 HFC. In the area of the G-3762 test corehole, high vuggy porosity in the bottom section of the Q4 HFC is developed best (Fig. 4). This high porosity at the G-3762 test corehole is expressed as a thick zone of relatively low amplitude reflections in the bottom section of the Q4 HFC on the GPR profile shown in Fig. 3. Comparison of Q4 HFC reflection amplitudes in Fig. 7a and b confirms that the reflection amplitudes at the top of the Q4 HFC are about 9 dB higher than at the base of the Q4 HFC. Formation conductivity in the top layers of the Q4 HFC is also

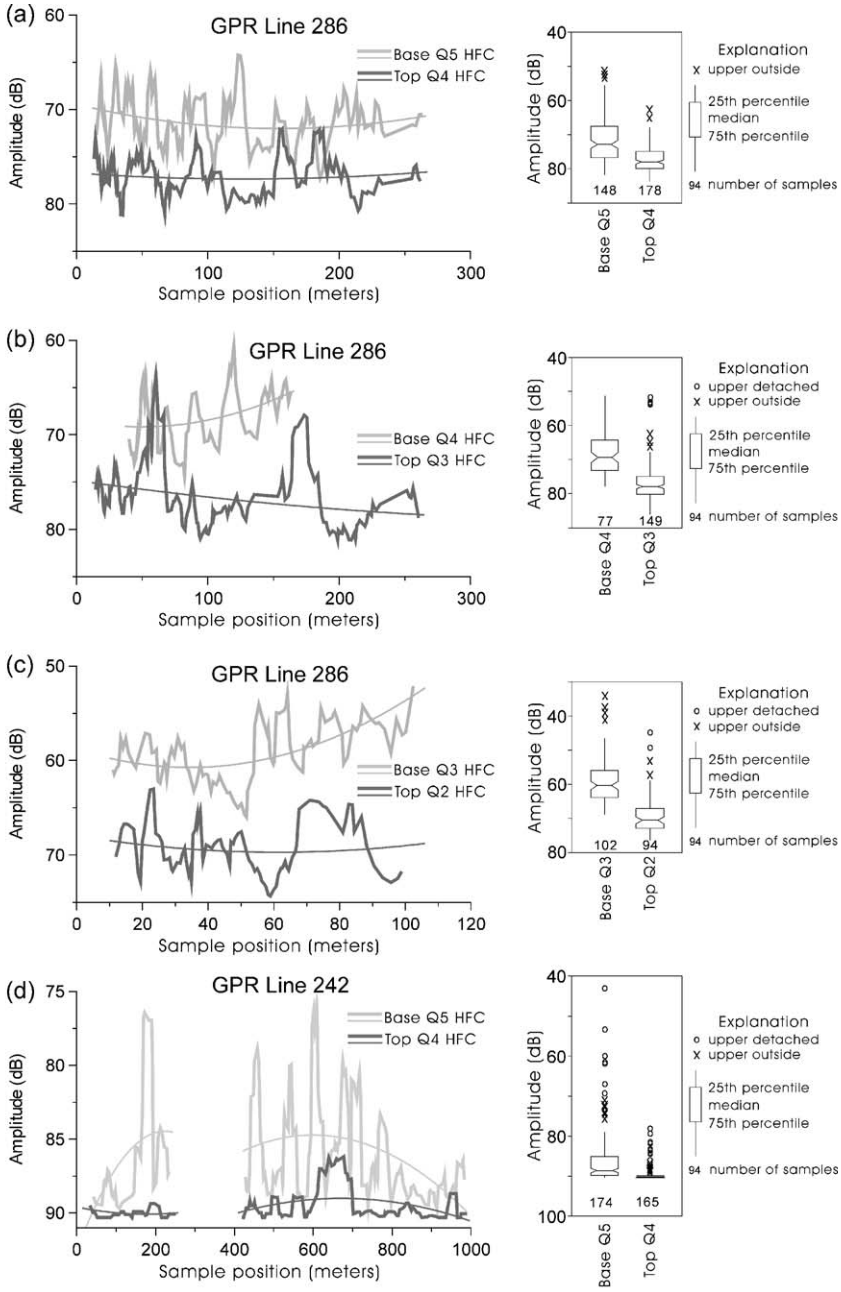

Fig. 7. Changes in ground-penetrating (GPR) reflection amplitudes over GPR survey distance, and corresponding box-whisker plots showing reflection amplitude sample populations for GPR reflection events at the base and tops of high-frequency cycles (HFCs). Uses data from GPR line 286 from the Rocky Glades site and GPR line 242 from the north-central Miami-Dade site. Reflection amplitudes at cycle bases are mostly lower than the reflection amplitudes from underlying cycle tops as shown by comparison of amplitude between (a, d) the base of Q5 high-frequency cycle (HFC) and top of Q4 HFC, (b) the base of cycle Q4 HFC and top of the Q3 HFC, and (c) the base of the Q3 HFC and the top of the Q2 HFC. Box-whisker plots show that there is a significant difference between median values of reflection amplitudes for values from contiguous cycle tops and cycle bases. The two very irregular curves in the graphs are based on running averages and the two smooth curves are based on a polynomial averaging. See Fig. 5 for an explanation of box-whisker plots.

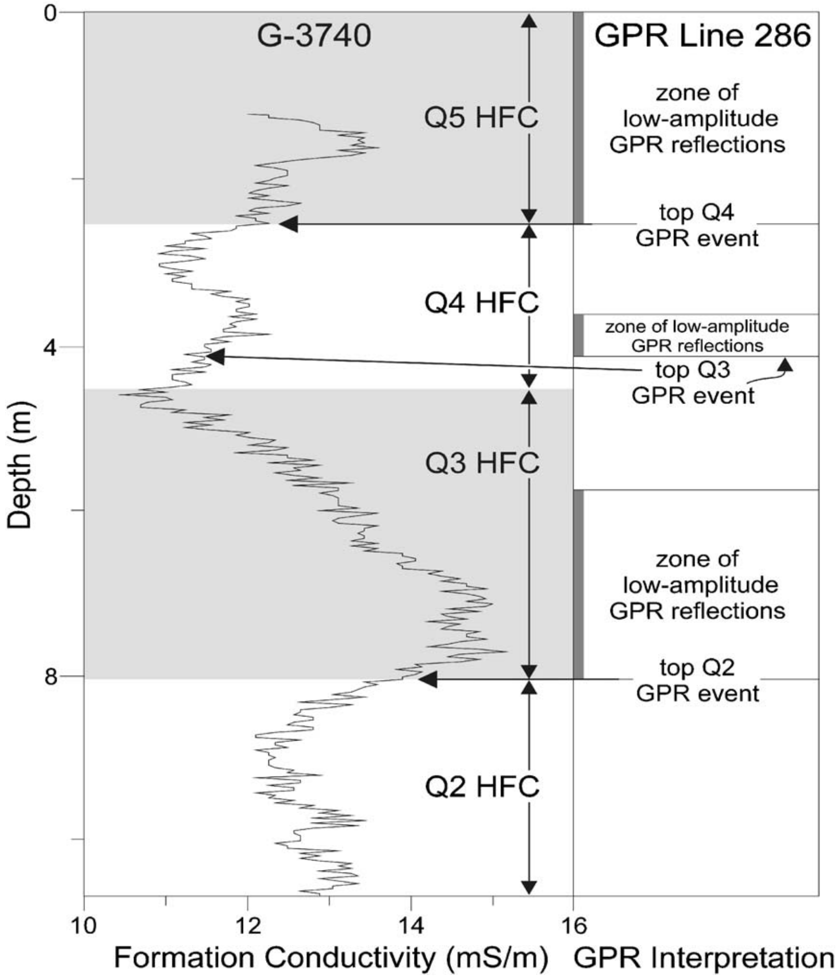

Fig. 8. Formation conductivity measured by an induction-resistivity borehole-geophysical tool for the G-3740 test corehole and ground-penetrating radar (GPR) events interpreted from GPR line 286 (Fig. 3). Zones of relatively higher electrical conductivity correspond to zones of relatively high vuggy porosity on digital optical borehole images and zones of relative low-amplitude reflections on the GPR line 286. High-frequency cycles (HFC) determined from stratigraphic analysis of cores and digital borehole images.

higher than in much of the bottom section of the cycle (Fig. 8).

The high water saturation of the thick zone of high vuggy porosity in the bottom section of the Q4 HFC near the G-3762 test corehole (Fig. 4) produces a velocity pulldown in the reflections of the upper surface of the Q3 HFC (Fig. 3). The velocity of EM waves in freshwater (0.033 m/ns) is considerably slower than that of limestone (0.12 m/ns) according to Davis and Annan (1989). The interval velocity between the ground surface and top layers of the Q4, Q3 and Q2 HFCs was determined by correlation of a CMP analysis (Fig. 9a) with layers identified in test corehole G-3740 (Fig. 3). The computed velocity, 0.06 m/ns, is about half of Davis and Annan's (1989) limestone velocity. The lower south Florida velocities are probably due to very high limestone porosity and almost complete ground saturation.

These data suggest that the apparent structural low on the upper surface of the Q3 HFC (Fig. 3) was caused by a relatively slow two-way traveltime of EM waves through the vuggy porosity zone. Correlation of the top of the Q3 GPR anomaly between the G-3740 and G-3762 test coreholes shows that

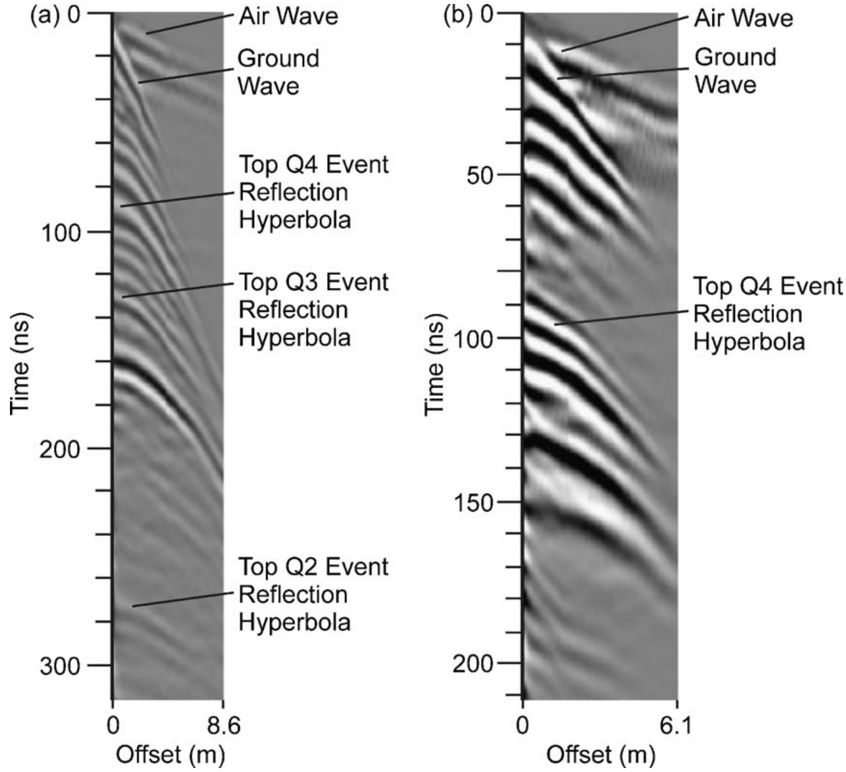

Fig. 9. Common mid-point velocity surveys. (a) Survey from due north of the G-3740 test corehole (Fig. 3) and (b) survey from near the G-3710 test corehole (Fig. 10).

there is almost no difference in the altitude of the Q3 GPR event between the test coreholes (Fig. 4). The roughly 1-m thick structural "sag" in the altitude of the top of the Q3 GPR event near the G-3762 corehole, is thus attributed to a decrease in velocity (Fig. 3). Further evidence of the velocity pulldown is the similar in vertical distance between the top Q4 GPR event and top Q3 GPR event at the G-3762 test corehole relative to the G-3740 test corehole (Fig. 4).

The GPR reflections at the tops of the Q3 and Q2 HFCs have amplitudes averaging about 9–11 dB higher than overlying reflections at the bases of the Q4 HFC and Q3 HFC, respectively (Fig. 7b and c). Low porosity lime mudstone and wackestone cap both the Q3 and Q2 HFCs (Fig. 4), whereas vuggy, pelecypod floatstone and rudstone compose the bases of these cycles. Fifty-three whole-core samples from the Q3 and Q2 peritidal HFCs from both the Rocky Glades GPR site and the Lake Belt Area (Fig. 1) confirm that porosity values decrease upward from the base to the tops of pertidal cycles (Fig. 5). Further, core-scale hydraulic conductivity values decrease upward from the base to the tops of peritidal cycles (Fig. 6). This upward trend in decreasing porosity and hydraulic conductivity reflects a decrease in grain size and an increase in matrix micrite upward within the HFCs, and is expressed as an upward decrease in conductivity within the Q3 HFC (Fig. 8). Similar to the Q4 HFC, the upper part of the Q3 HFC has higher reflection amplitudes than the lower part of the Q3 HFC (Figs. 3 and 7) that are apparently related to an upward decrease in porosity and freshwater saturation. The highly porous zones in the Q4 and Q3 HFCs (Fig. 4) could be a laterally well-connected, incipient dissolutional cave system that is similar to more evolved cave systems described by Ford (1988).

5.2. North-central Miami-Dade site

Two high-frequency carbonate cycles (Q5 and Q4 HFCs) of the Miami Limestone and the uppermost high-frequency cycle (Q3b HFC) of the Fort Thompson Formation are imaged on GPR profile 242, which was collected at the north-central Miami-Dade GPR site (Figs. 1, 2 and 10). A thin calcrete layer at the top of each HFC provides evidence that a surface of subaerial exposure, which was related to a relative fall in sea level, caps each HFC (Fig. 11). A prominent karstic exposure surface that shows evidence for significant dissolution along the surface separates HFCs Q5 and Q4, as shown in Fig. 11. This buried karstic surface has up to 1 m of paleorelief and, locally, karstic dissolution has almost entirely removed the Q4 HFC (Figs. 10 and 11). Digital optical borehole images and continuously drilled cores confirm that the Q4 HFC is relatively thick to almost absent (Fig. 11). Verification of the interpretation shown in Fig. 10 would not have been possible with only cores because of incomplete recovery and the associated error in depths. Only with the digital optical borehole images (Fig. 11) was it possible to verify unambiguously the interpretation shown in Fig. 10.

Typical reflection configuration patterns and lithofacies in the Q5 HFC are like those described earlier for the Q5 HFC at the Rocky Glades site. Fig. 10 shows that the GPR reflections of the Q5 HFC are lower amplitude than reflections of the Q4 HFC and upper part of the Q3b HFC. Comparison of amplitudes of a GPR reflection at the base of the Q5 HFC and a reflection at the top of the Q4 HFC indicate that the median amplitude of the Q5 HFC reflection is about 7 dB less than the upper reflection of the Q4 HFC (Fig. 7d). This difference is significant at about a 95% confidence level (Fig. 7d). The relatively low amplitudes of the Q5 reflections are probably related to a very high pelmoldic matrix porosity and solution-enlarged burrow porosity, which are characteristic of the Q5 HFC, relative to lower matrix porosity (Fig. 5) and more micrite-rich peloidal facies of the Q4 HFC. These relations between the GPR reflection amplitudes and porosity of the Q5 HFC, and the amplitudes and porosity of the Q4 HFC are almost ubiquitous in the data collected at the Rocky Glades GPR site and throughout the Lake Belt Area (Fig. 1). Relatively low-amplitude reflections assigned to the Q5 HFC shown in Fig. 10 correspond to a zone of relatively high formation conductivity in test corehole G-3713 (Fig. 12). This observation corroborates the empirical relation between porosity, hydraulic conductivity, formation conductivity, and reflection amplitudes—as porosity increases, hydraulic conductivity and formation conductivity increases, and reflection amplitude decreases.

The interval velocity between the ground surface and top of the Q4 HFC is 0.06 m/ns as determined by CMP analyses near test coreholes G-3710 and G-3711 at the north-central Miami-Dade site (Figs. 9b and

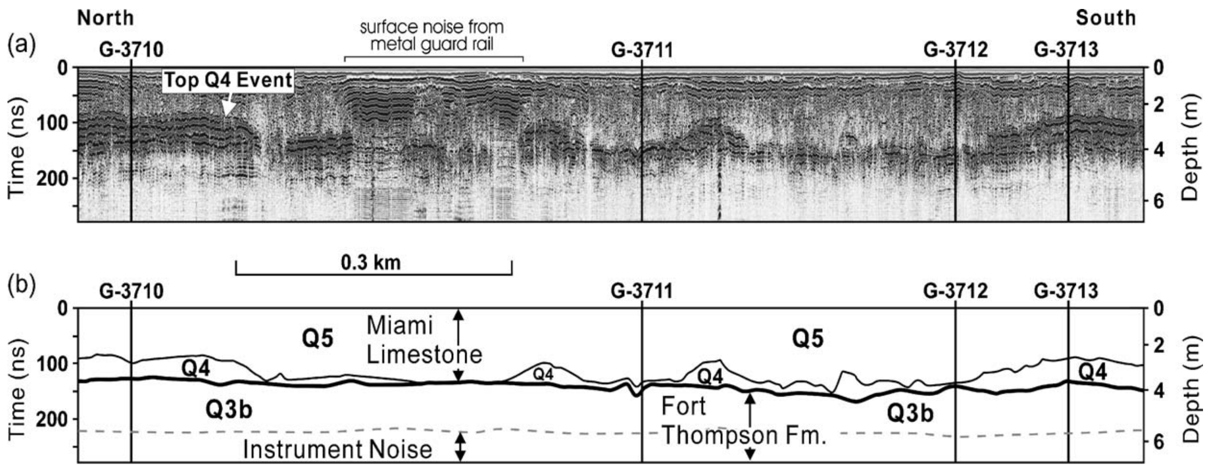

Fig. 10. Ground-penetrating radar (GPR) line 242 at the north-central Miami-Dade GPR site. (a) 100-MHz GPR profile. (b) Line drawing of GPR profile. Q5, Q4 and Q3b correspond to the high-frequency cycle stratigraphy shown in Fig. 2.

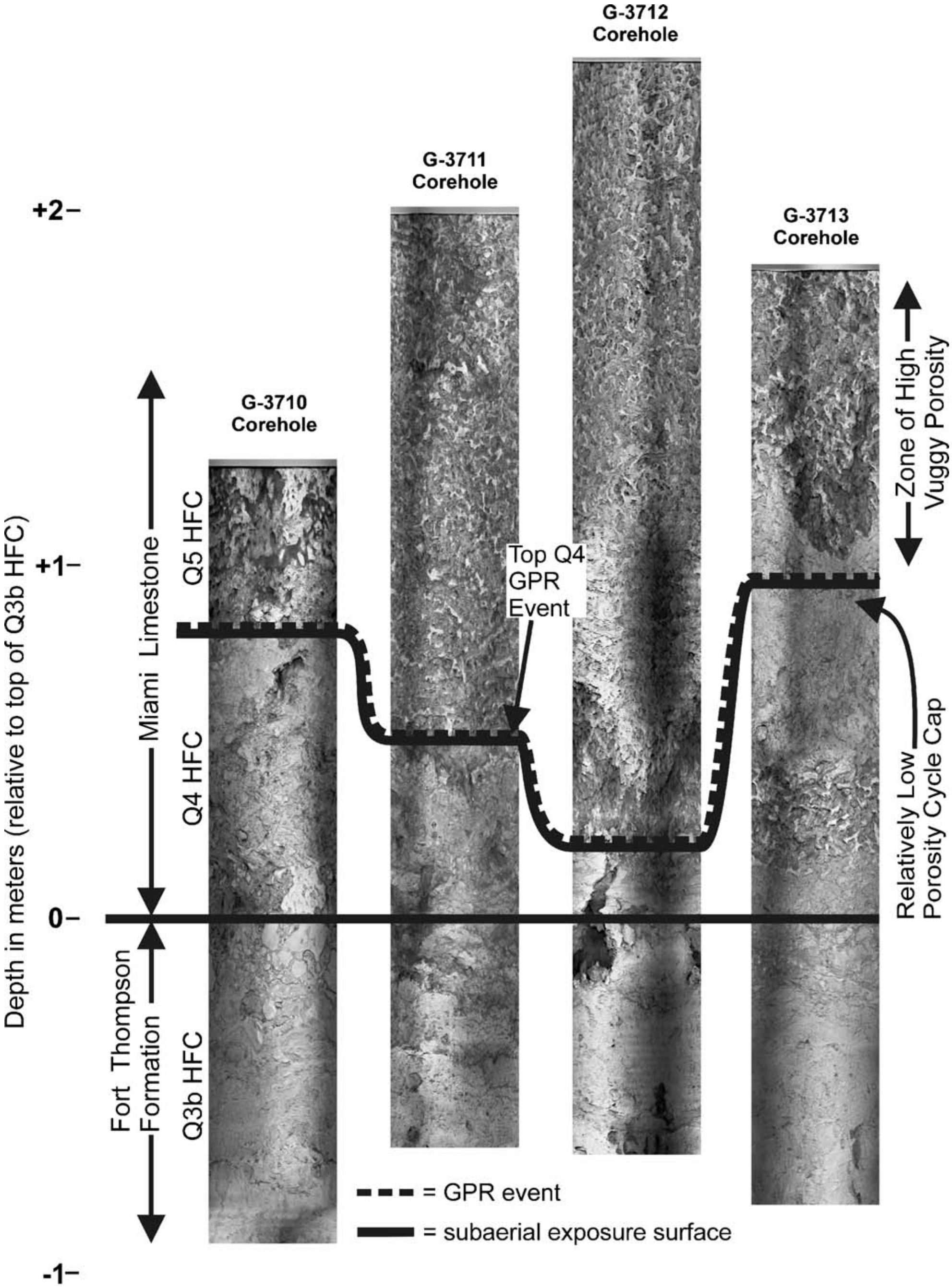

Fig. 11. Correlation of four digital optical borehole image logs from test coreholes G-3710, G-3711, G-3712, and G-3713 used to verify ground-penetrating radar at the north-central Miami-Dade GPR site (Fig. 10).

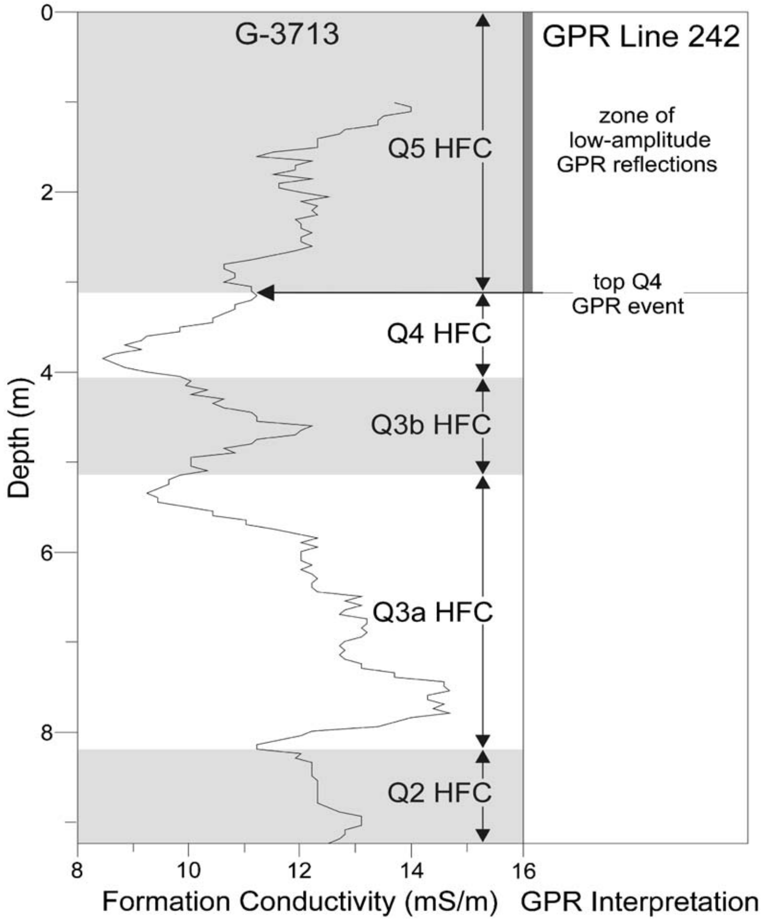

Fig. 12. Formation conductivity measured by an induction-resistivity borehole-geophysical tool for the G-3713 test corehole and ground-penetrating radar (GPR) events interpreted from GPR line 242 (Fig. 10). The zone of relatively high electrical conductivity within the Q5 high-frequency cycle (HFC) corresponds to a vertical and lateral zone of relatively low-amplitude reflections assigned to the Q5 HFC shown on the ground-penetrating radar line 242 (Fig. 10). High-frequency cycles determined from stratigraphic analysis of cores and digital borehole images.

10). This velocity is the same as the velocity determined at the Rocky Glades site and similar to a velocity (0.05 m/ns) calculated by Kruse et al. (2000) for the limestone of the upper Biscayne aquifer in an area of Everglades National Park (ENP).

6. Discussion and conclusions

Ground-penetrating radar (GPR) is a useful tool in the hydrogeologic characterization of shallow carbonate aquifers. This technique was applied to karstic Pleistocene platform carbonates of the upper Biscayne aquifer in southeastern Florida. Geologic features shown on resultant GPR profiles include: (1) two-dimensional, qualitative distribution of porosity on hydraulic conductivity; (2) paleotopographic relief on karstic subaerial exposure surfaces; and (3) vertical stacking of chronostratigraphic high-frequency cycles (HFCs). These characteristics were verified by comparison to rock properties observed and measured in rock samples from continuously drilled cores, and identified in digital optical borehole images.

An empirical relation exists between measured whole-core porosity, observed porosity on digital optical borehole images, formation conductivity, and GPR reflection amplitudes—as porosity determined from core and images increases, formation conductivity increases, and reflection amplitude decreases. A plausible explanation is that attenuation of GPR-EM waves increases as the freshwater saturation of the medium increases. Borehole-conductivity logs show that highly porous limestone of the Biscayne aquifer with relatively high freshwater saturation has a higher conductivity than low-porosity limestone with relatively low freshwater saturation. Thus the highly porous, highly conductive zones within the limestone of the Biscayne aquifer have low reflection amplitude, because as the electrical conductivity of a medium increases the attenuation of the GPR-EM waves increases.

The stratigraphic framework of the uppermost part of the Biscayne aquifer is composed of two high-frequency subtidal carbonate cycles that form the Miami Limestone. Whole-core porosity values from the upper subtidal HFC are typically about two to three times higher than whole-core porosity measurements from the underlying subtidal HFC. GPR profiles show that overall, the higher porosity of the upper HFC generates lower amplitude reflections than the underlying lower porosity HFC. Also, measured basal reflection amplitudes of the upper subtidal HFC are significantly lower than measured reflection amplitudes of the lower subtidal HFC.

The Fort Thompson Formation underlies the Miami Limestone and forms the middle to lower part of the Biscayne aquifer. The upper Fort Thompson Formation is composed of multiple high-frequency peritidal carbonate cycles. Porosity values measured from whole-core samples show that the lowest porosity occurs at HFC tops, moderate porosity at the middle of the HFCs, and the highest porosity at the base of the HFCs. This change in porosity from bottom to top is visible as an upward variation in reflection amplitude on GPR profiles—lowest amplitudes at the base and highest at the HFC tops. Using a 100-MHz source, amplitudes of reflections of relatively low-porosity cycle tops typically have median values about 2–11 dB higher than amplitudes of reflections in overlying relatively high-porosity cycle bases.

This study demonstrates that GPR can be used to show the qualitative distribution of porosity within a cycle-stratigraphic framework composed of carbonate HFCs. The distribution of porosity within HFCs is mostly controlled by depositional textures. The upward and lateral patterns of rock facies within the HFCs can be translated to borehole geophysical properties and radar facies configurations that could aid in interpretation and prediction of ground-water flow through a carbonate aquifer. Furthermore, the highly porous zones identified in HFCs at the Rocky Glades site could be a laterally well connected, incipient dissolutional cave system that is similar to more evolved cave systems described by Ford (1988).

Acknowledgements

This project was funded by the South Florida Water Management District and Critical Ecosystems Studies Initiative. Robert Zepp is thanked for permits to drill in the ENP. Bill Loftus, Sue Perry, and Cristina Bruno are thanked for initiating the ENP portion of the project. Anthony Brown, Jean-Claude Poix, David Schmerge, Marc Stewart, and Diane Riggs assisted with field activities. Peter Joesten, Ron Reese, John Lane, and Carole Johnson are thanked for early critical reviews. The Branch of Geophysics, USGS, provided essential geophysical instrumentation.

References

Annan, A.P., Davis, J.L., 1976. Impulse radar soundings in permafrost. Radio Science 11, 383–394.

Ballard, R.F., 1983. Electromagnetic (radar) techniques applied to cavity detection. U.S. Army Corps of Engineers Water Way Experimental Station Technical Report GL-83-1, Report 5. 90 pp.

Barr, G.L., 1993. Applications of ground penetrating radar methods in determining hydrogeologic conditions in a karst area, west-central Florida. U.S. Geol. Surv. Water-Resources Invest. Report 92-4141. 26 pp.

Beck, B.F., Wilson, W.L., 1988. Interpretion of ground penetrating radar profiles in karst terrane. Proceedings of the Second Conference on Environmental Problems in Karst Terranes and their Solutions, Nashville, TN, November 16–18, 1988. National Water Well Association, pp. 347–367.

Beres Jr., M., Haeni, F.P. 1991. Application of ground-penetrating radar methods in hydrogeologic studies. Ground Water 29, 375–386.

Beres, M., Luester, M., Olivier, R., 2001. Integration of ground-penetrating radar and microgravimetric methods to map shallow caves. J. Appl. Geophys. 46, 249–262.

Causaras, C.R., 1987, Geology of the surficial aquifer system, Dade County, Florida. U.S. Geol. Surv. Water-Resources Invest. Report 86-4126. 240 pp., 3 sheets.

Cunningham, K.J., Aviantara, A., 2001. Characterization of the karstic Biscayne aquifer in southeastern Florida using ground-penetrating radar, digital optical borehole images and core (abstract), In: Kuniansky, E.L. (Ed.), U.S. Geological Survey Karst Interest Group Proceedings St. Petersburg, Florida, February 13–16, 2001. U.S. Geol. Surv. Water-Resources Invest. Report 01-4011, p. 134.

Dagallier, G., Laitinen, A.I., Malartre, F., Van Campenhout, I.P.A.M., Veeken, P.C.H., 2000. Ground penetrating radar application in a shallow marine Oxfordian limestone sequence located on the eastern flank of the Paris Basin, NE France. Sediment. Geol. 130, 149–165.

Davis, J.L., Annan, A.P., 1989. Ground-penetrating radar for high-resolution mapping of soil and rock stratigraphy. Geophys. Prospect. 37, 531–551.

Fish, J.E., Stewart, M., 1991. Hydrogeology of the surficial aquifer system, Dade County, Florida: U.S. Geol. Surv. Water-Resources Invest. Report 90-4108. 50 pp.

Ford, D., 1988. Characteristics of dissolutional cave systems in carbonate rocks. In: James, N.P., Choquette, P.W. (Eds.), Paleokarst. Springer-Verlag, New York, pp. 25–57.

Grasmueck, M., 1996. 3-D ground-penetrating radar applied to fracture imaging in gneiss. Geophysics 61, 1050–1064.

Johnson, D.G., 1992. Use of ground-penetrating radar for water-table mapping, Brewster and Harwick, Massachusetts. U.S. Geol. Surv. Water-Resources Invest. Report 90-4086. 27 pp.

Kruse, S.E., Schneider, J.C., Campagna, D.J., Inman, J.A., Hickey, T.D., 2000. Ground penetrating radar imaging of cap rock, caliche and carbonate strata. J. Appl. Geophys. 43, 239–249.

Lane Jr., J.W., Buursink, M.L., Haeni, F.P., Versteeg, R.J., 2000. Evaluation of ground-penetrating radar to detect free-phase hydrocarbons in fractured rocks—results of numerical modeling and physical experiments. Ground Water 38, 929–938.

Lucia, F.J., 1999. Carbonate Reservoir Characterization. Springer-Verlag, Berlin. 226 pp.

Martinez, A., Kruger, J.M., Franseen, E.K., 1998. Utility of ground-penetrating radar in near-surface, high-resolution imaging of Lansing-Kansas City (Pennsylvanian) Limestone reservoir analogs. Current Research in Earth Sciences. Kansas Geol. Surv. Bull., vol. 241, part 3, pp. 43–59.

McMechan, G.A., Loucks, R.G., Zeng, X., Mescher, P., 1998. Ground penetrating radar imaging of a collapsed paleocave system in the Ellenburger dolomite, central Texas. J. Appl. Geophys. 39, 1–10.

Mitchum Jr., R.M., Vail, P.R., Sangree, J.B., 1977. Seismic stratigraphy and global changes of sea level, part 6: stratigraphic interpretation of seismic reflection patterns in depositional sequences. In: Payton, C.E. (Ed.), Seismic Stratigraphy—Applications to Hydrocarbon Exploration. Amer. Assoc. Petrol. Geol. Mem., vol. 26, pp. 117–133.

Perkins, R.D., 1977. Depositional framework of Pleistocene rocks in south Florida. In: Enos, P., Perkins, R.D (Eds.), Quaternary Sedimentation in South Florida, Part II. Geol. Soc. Am. Mem., vol. 147, pp. 131–198.

Smith, D.G., Jol, H.M., 1992. Ground-penetrating radar investigation of a Lake Bonneville delta, Provo level, Brigham City, Utah. Geology 20, 1083–1086.

van Overmeeren, R.A., 1998. Radar facies of unconsolidated sediments in The Netherlands: a radar stratigraphy interpretation method for hydrogeology. J. Appl. Geophys. 40, 1–18.